## PAPER

# Dye-sensitized solar cells with hole-stabilizing surfaces: "inorganic" *versus* "organic" strategies†

Nik Hostettler, Iain A. Wright, Biljana Bozic-Weber, Edwin. C. Constable* and Catherine E. Housecroft*

Two 2,2':6',2''-terpyridine ligands (**9** and **10**) incorporating second-generation diphenylamino-dendrons have been synthesized and characterized; one ligand contains chromophoric benzothiadiazole domains. Using the 'surface-as-ligand, surface-as-complex' strategy, zinc(II)-containing sensitizers [Zn(L$_{anchor}$)(L$_{ancillary}$)]$^{2+}$ with carboxylic or phosphonic acid anchors (**1** and **2**, respectively) have been assembled and tested in n-type DSCs. The solid-state absorption spectra of dye-functionalized electrodes show a broad spectral response for all the dyes with enhanced intensity for those containing the benzothiadiazole units. However, the [Zn(L$_{anchor}$)(L$_{ancillary}$)]$^{2+}$ dyes perform poorly, exhibiting very low values of the short-circuit current density ($J_{SC}$) and open-circuit voltage ($V_{OC}$). The external quantum efficiency (EQE) spectra confirm that electron injection occurs, but EQE$_{max}$ is ≤3%. Non-optimal positioning of the thiadiazole domain in the dye probably contributes to the poor performances. Screening of DSCs containing FTO/TiO$_2$ photoanodes *without* adsorbed dye shows that they generate small short-circuit current densities and open-circuit voltages which contribute significantly to parameters reported for badly performing dyes. An organic dye **11**, structurally similar to **10** and containing a 2-cyanoacrylic acid anchor, is also reported. This exhibits a broad and intense spectral response between 300 and 600 nm, and shows efficient electron injection over a broad wavelength range. DSCs containing **11** are stable over a 17 day period and show global efficiencies of 3.93–4.57% (*ca.* 70% with respect to N719 set at 100%). Ground state DFT calculations reveal that the HOMO in each of [Zn(**1**)(**9**)]$^{2+}$, [Zn(**2**)(**9**)]$^{2+}$, [Zn(**1**)(**10**)]$^{2+}$, [Zn(**2**)(**10**)]$^{2+}$ and **11** is localized on the peripheral diphenylamino units, allowing for hole-transfer to the reduced electrolyte. In **11**, a major contribution from the 2-cyanoacrylic acid anchoring group appears in the LUMO manifold; however, while the LUMO in each zinc(II) dye is localized on anchoring ligand **1** or **2**, it is concentrated close to the metal centre which may contribute to poor electron injection.

## Introduction

Dye-sensitized solar cells (DSCs) were developed around twenty years ago and, even at an early stage, exhibited relatively high efficiencies.[1] Improvements in DSC design have increased the efficiency of the conversion of photons to electrical current.[2,3] Conversion efficiency depends on optimizing the photo-response of the dye, the electron injection, and the rate of oxidized dye regeneration. It is also essential to minimize charge recombination events.[4–6] In a Grätzel n-type DSC, the LUMO of the dye must be higher than the level of the TiO$_2$ conduction band[7] (−4.0 eV), while the HOMO of the dye should be slightly lower than the HOMO of the redox couple (−4.9 eV for the archetypal I$^-$/I$_3^-$ redox shuttle).[8] Design of transition

metal-containing sensitizers and molecular organic dyes must take account of all the above criteria.[3,9]

We and others are developing sensitizers for DSCs which incorporate low cost Earth-abundant metals to replace rare elements such as ruthenium.[10] Copper(I) sensitizers[11–26] feature strongly, but we have also reported the successful use of {Zn(tpy)$_2$}$^{2+}$-containing dyes (tpy = 2,2':6',2''-terpyridine), albeit with low photon-to-current conversion efficiencies.[27,28] The lability of both copper(I) and zinc(II) complexes permits sequential assembly of photoactive dyes on a semiconductor surface using the 'surface-as-ligand, surface-as-complex' methodology;[17] ligand exchange is rapid for copper(I) but slower for zinc(II). Fig. 1 summarizes the strategy for {Zn(tpy)$_2$}$^{2+}$ sensitizers, involving initial treatment of an FTO/TiO$_2$ surface with an anchoring tpy ligand (*e.g.* **1** and **2**, Scheme 1), followed by treatment of the surface-as-ligand with a zinc(II) salt, and finally reaction of the surface-as-complex with a chromophore-functionalized tpy ancillary ligand such as **3–7** (Scheme 1).[27] Although ligand exchange in [Zn(tpy)$_2$]$^{2+}$ complexes is slow on the NMR timescale,[27] once assembled, [Zn(tpy)$_2$]$^{2+}$ domains anchored to the n-type semiconductor are stable. This stepwise

*Department of Chemistry, University of Basel, Spitalstrasse 51, CH-4056 Basel, Switzerland. E-mail: catherine.housecroft@unibas.ch*
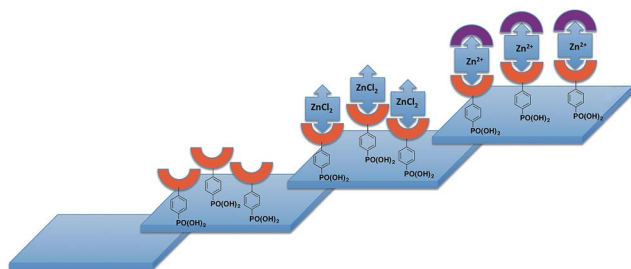
Fig. 1 Assembly of zinc(II)-complexes in a stepwise manner using the 'surface-as-ligand, surface-as-complex' methodology in which the FTO/TiO$_2$ surface (blue) is sequentially functionalized with an anchoring ligand (exemplified with a phosphonic acid anchoring domain, red = tpy metal-binding domain), metallated with ZnCl$_2$, and finally capped by an ancillary ligand (purple).

procedure contrasts with the preparation of heteroleptic dyes by the HETPHEN[29] approach,[19,21] or by the use of ligand exchange reactions involving homoleptic metal complexes.[10] Advantages of the *in situ* stepwise strategy are a reduction in the number of synthetic steps in dye preparation and a consequential atom and financial economy[16,17] for the photoactive materials.

Unlike copper(I)-containing dyes which exhibit metal-to-ligand charge transfer (MLCT) bands in the visible region, zinc(II) complexes characteristically possess absorption spectra dominated by intra-ligand transitions. In sensitizers based on {Zn(tpy)$_2$} complexes, the zinc(II) ion acts as 'glue' between the anchoring and ancillary ligand domains. The advantage of the assembly principle shown in Fig. 1 is that it facilitates screening of a wide range of ligand combinations. In order that the photoresponse of the dye incorporates the visible region, it is essential that the ancillary ligand contains a chromophore. Consequently, the formation of the surface-bound {Zn(tpy)$_2$} unit is readily monitored by an optical change.[27,28]

In contrast to the highly promising performance of porphyrinato zinc(II) dyes which can achieve power conversion efficiencies of up to 13%,[30,31] DSCs containing {Zn(tpy)$_2$} complexes with anchoring ligands **1** and **2**, and ancillary ligands **3–7**[27,28] exhibit very low efficiencies, in part due to inadequate light-harvesting in the visible. A common strategy for enhancing light absorption is by extending the π-conjugation[32] or by combining electron-donating and electron-accepting moieties in the same conjugated ligand framework (so called 'push–pull' dyes).[33] Here, we report the development of {Zn(tpy)$_2$} sensitizers by moving from first generation ligands **3–7** to second generation analogues **8** and **9**, and to the related
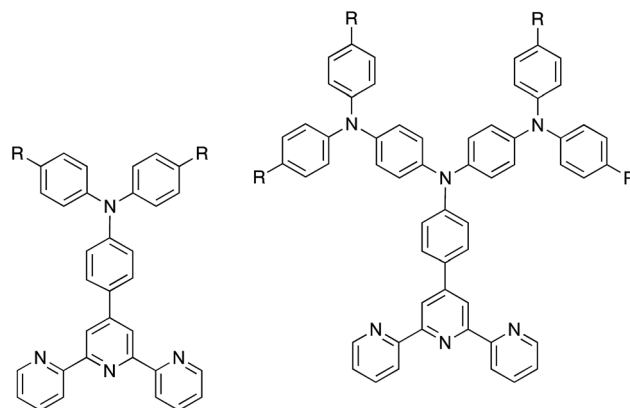


Scheme 2 The structures of first-generation ancillary ligands **3–7**, second generation ligands **8–10**, and organic dye **11**.

ligand **10** which contains a benzothiadiazole spacer (Scheme 2). The chromophoric benzothiadiazole unit is well-established in organic dyes; its electron-withdrawing characteristics result in a red-shift in the absorption maximum with respect to analogous dyes without this domain.[32–36]

## Experimental

### General

A Bruker Avance III-500 NMR spectrometer was used to record $^1$H and $^{13}$C NMR spectra, and chemical shifts were referenced to
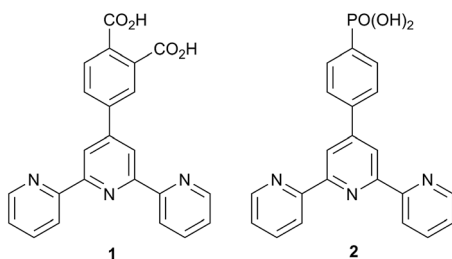


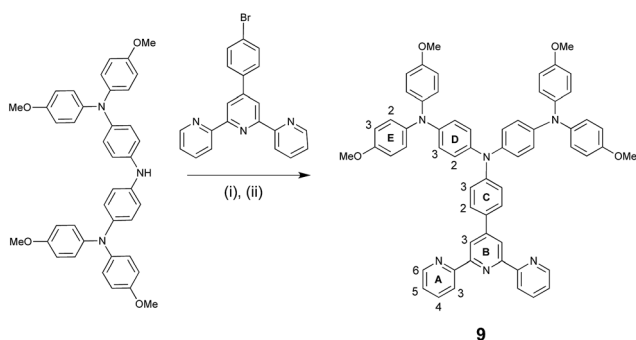Scheme 1 Anchoring ligands **1** and **2** for {Zn(tpy)$_2$}$^{2+}$-containing dyes.

residual solvent peaks with respect to $\delta$(TMS) = 0 ppm. MALDI-TOF mass spectra were recorded on Bruker Daltonics microflex instrument and electrospray ionization (ESI) mass spectra and high-resolution ESI mass spectra were measured using Bruker esquire 3000$^{plus}$ and Bruker maXis 4 G mass spectrometers. Solution absorption spectra were recorded with a Cary 5000 spectrophotometer and FT-IR spectra of solid samples on a Perkin Elmer UATR Two spectrometer. Electrochemical measurements were made using a CH Instruments 900B potentiostat with glassy carbon, platinum wire and silver wire as the working, counter, and reference electrodes, respectively. Samples were dissolved in HPLC grade $CH_2Cl_2$ ($10^{-4}$ to $10^{-5}$ mol dm$^{-3}$) containing 0.1 mol dm$^{-3}$ [$^nBu_4N$][$PF_6$] as the supporting electrolyte; all solutions were degassed with argon.

Compound **1**,[27] 4′-(4-bromophenyl)-2,2′:6′,2″-terpyridine[37] and 4,4′-bis(N,N-bis(4-methoxyphenyl)amino)diphenylamine[11] were prepared as previously described, and compound **2** was supplied by M. Waser, FHNW, Basel. The syntheses of bis(4-(7-(diphenylamino)benzo[c][1,2,5]thiadiazol-4-yl)phenyl)amine (**10a**, Scheme 4) and 4-(bis(4-(7-(diphenylamino)benzo[c][1,2,5]-thiadiazol-4-yl)phenyl)amino) benzaldehyde (Scheme 5) are described in the ESI.† Bis(dibenzylideneacetone)palladium(0), [Pd(dba)$_2$] was purchased from Strem Chemicals.
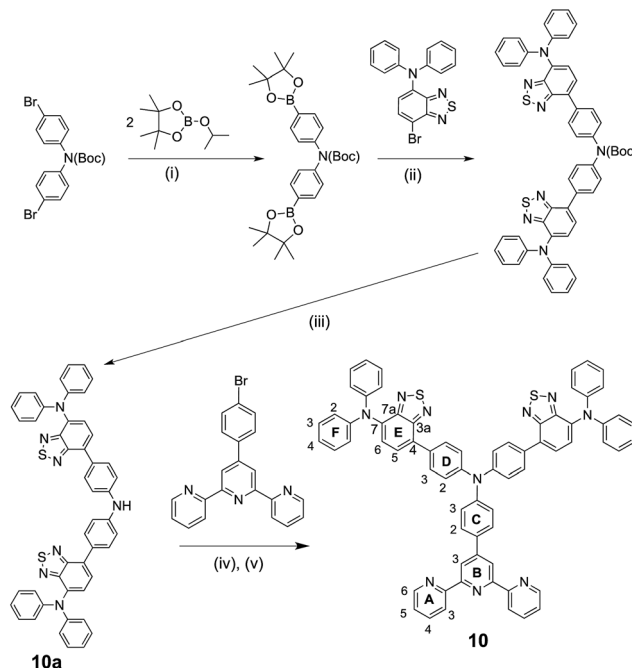
Ground state density functional theory (DFT) calculations were performed using Spartan 14 (v. 1.1.8)[38] at the B3LYP level with a 6-31G* basis set in vacuum. Initial structure minimization was carried out at a molecular mechanics or PM3 level.

## Compound 9

Solid 4,4′-bis(N,N-bis(4-methoxyphenyl)amino)diphenylamine (150 mg, 0.234 mmol), 4′-(4-bromophenyl)-2,2′:6′,2″-terpyridine (83.2 mg, 0.214 mmol), NaO$^t$Bu (67.9 mg, 0.707 mmol) and a catalytic amount of [Pd(dba)$_2$] (4.93 mg, 8.57 µmol) were placed in a flask under N$_2$. Dry degassed toluene (10 mL) and P$^t$Bu$_3$ (8.57 µL 1 M solution in toluene, 8.57 µmol) were then added. The mixture was stirred for 3 days at 100 °C. The solvent was then removed under reduced pressure and the solid residue was recrystallized from acetone. The yellow solid was dissolved in CH$_2$Cl$_2$ (30 mL), washed with 6 M aqueous KOH (2 × 15 mL) and H$_2$O (3 × 20 mL), and then dried over MgSO$_4$. The solvent was removed under reduced pressure and **9** was isolated as a pale
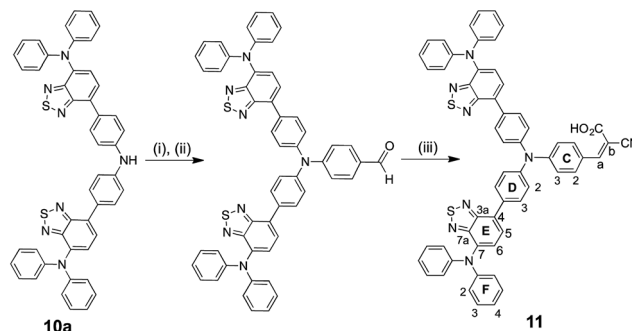


**Scheme 4** Synthetic route to compound **10**. Conditions: (i) $^nBuLi$, THF, −78 °C warming to room temperature; (ii) K$_2$CO$_3$, H$_2$O/THF; Pd(PPh$_3$)$_4$, reflux, 3 days; (iii) 210 °C, 1 h, no solvent; (iv) NaO$^t$Bu; (v) [Pd(dba)$_2$], P$^t$Bu$_3$, toluene, 100 °C, 16 h.

yellow solid (95.0 mg, 0.102 mmol, 47.7%). $^1$H NMR (500 MHz, THF-$d_8$) $\delta$/ppm 8.81 (s, 2H, H$^{B3}$), 8.70 (m, 2H, H$^{A3}$), 8.67 (ddd, $J$ = 4.8, 1.8, 0.9 Hz, 2H, H$^{A6}$), 7.89 (td, $J$ = 7.7, 1.8 Hz, 2H, H$^{A4}$), 7.75 (m, 2H, H$^{C2}$), 7.35 (ddd, $J$ = 7.5, 4.7, 1.2 Hz, 2H, H$^{A5}$), 7.11 (m, 2H, H$^{C3}$), 7.04 (m, 8H, H$^{E2}$), 7.01 (m, 4H, H$^{D2}$), 6.88 (m, 4H, H$^{D3}$), 6.83 (m, 8H, H$^{E3}$), 3.75 (s, 12H, H$^{OMe}$). $^{13}$C NMR (126 MHz, THF-$d_8$) $\delta$/ppm 157.2 (C$^{A2}$), 157.1 (C$^{E4}$), 156.9 (C$^{B2}$), 150.7 (C$^{C1/C4}$), 150.5 (C$^{C1/C4}$), 150.0 (C$^{A6}$), 146.2 (C$^{D4}$), 142.1 (C$^{E1}$), 141.1 (C$^{D1}$), 137.4 (C$^{A4}$), 130.9 (C$^{B4}$), 128.5 (C$^{C2}$), 127.1 (C$^{E2}$), 124.6 (C$^{A5}$), 122.7 (C$^{D3}$), 121.6 (C$^{A3}$), 121.4 (C$^{C3}$), 118.4 (C$^{B3}$), 115.5 (C$^{E3}$), 55.6 (C$^{OMe}$). UV-Vis (THF, 2.4 × 10$^{-5}$ M) $\lambda_{max}$/nm ($\varepsilon$/dm$^3$ mol$^{-1}$ cm$^{-1}$) 296 (44 700), 335 sh (29 800), 382 sh (19 200). ESI-MS positive mode: $m/z$ 930.9 [M + H]$^+$ (calc. 931.4). MALDI-TOF MS $m/z$ 931.1 [M + H]$^+$ (calc. 931.4). HR ESI-MS positive mode: $m/z$ 930.3884



**Scheme 3** Synthetic route to compound **9**. Conditions: (i) NaO$^t$Bu; (ii) [Pd(dba)$_2$], P$^t$Bu$_3$, toluene, 100 °C, 20 h.



**Scheme 5** Synthetic route to compound **11**. Conditions: (i) NaO$^t$Bu, 4-bromobenzaldehyde, [Pd(dba)$_2$]; (ii) P$^t$Bu$_3$, toluene, 100 °C, 20 h; (iii) cyanoacetic acid, piperidine, MeCN, reflux 4 days.

[M]$^+$ (calc. 930.3888), 953.3778 [M + Na]$^+$ (calc. 953.3786). Satisfactory elemental analysis could not be obtained.

## Compound 10

Bis(4-(7-(diphenylamino)benzo[c][1,2,5]thiadiazol-4-yl)phenyl) amine (**10a** ESI†) (100 mg, 0.130 mmol), 4′-(4-bromophenyl)-2,2′:6′,2″-terpyridine (55.3 mg, 0.142 mmol), NaO$^t$Bu (37.3 mg, 0.389 mmol) and [Pd(dba)$_2$] (1.50 mg, 2.59 μmol) were placed in a flask under N$_2$. Dry degassed toluene (10 mL) and P$^t$Bu$_3$ (2.60 μL 1 M solution in toluene, 2.60 μmol) were added and the mixture was stirred overnight ($\approx$16 h) at 100 °C. The hot reaction mixture was then filtered through a glass frit, which was subsequently rinsed with hot toluene. The combined solvents were removed from the filtrate under reduced pressure and the solid residue was recrystallized from acetone. Compound **10** was obtained as a red solid (40.0 mg, 37.1 μmol, 29%). $^1$H NMR (500 MHz, CD$_2$Cl$_2$) δ/ppm 8.78 (s, 2H, H$^{B3}$), 8.72 (ddd, $J$ = 4.7, 1.7, 0.9 Hz, 2H, H$^{A6}$), 8.69 (m, 2H, H$^{A3}$), 7.95 (m, 4H, H$^{D3}$), 7.90 (overlapping m, 4H, H$^{A4+C2}$), 7.66 (d, $J$ = 7.8 Hz, 2H, H$^{E5}$), 7.41–7.35 (overlapping m, 8H, H$^{A5+D2+C3}$), 7.30–7.25 (overlapping m, 10H, H$^{E6+F3}$), 7.11–7.05 (m, 12H, H$^{F2+F4}$). $^{13}$C NMR (126 MHz, CD$_2$Cl$_2$) δ/ppm 156.6 (C$^{A2+B2}$), 155.3 (C$^{E3a}$), 152.2 (C$^{E7a}$), 149.9 (C$^{C1}$), 149.6 (C$^{A6}$), 148.7 (C$^{C4}$), 148.2 (C$^{F1}$), 147.4 (C$^{D1}$), 139.1 (C$^{E4}$), 137.3 (C$^{A4}$), 133.2 (C$^{B4}$), 132.9 (C$^{E7}$), 130.5 (C$^{D3}$), 129.4 (C$^{F3}$), 128.7 (C$^{C2}$), 128.4 (C$^{E5}$), 124.8 (C$^{D2+C3}$), 124.7 (C$^{E6}$), 124.4 (C$^{F2}$), 124.3 (C$^{A5}$), 123.6 (C$^{F4}$), 121.5 (C$^{A3}$), 118.5 (C$^{B3}$), (C$^{D4}$ not resolved). UV-Vis (CH$_2$Cl$_2$, 3 × 10$^{-6}$ M) λ$_{max}$/nm ($\varepsilon$/dm$^3$ mol$^{-1}$ cm$^{-1}$) 247 (51 200), 252 (51 500), 304 (62 200), 366 sh (21 500), 488 (23 000); (THF, 3 × 10$^{-5}$ M) 302 (70 600), 334 sh (40 600), 365 sh (27 500), 489 (26 100). MALDI-TOF MS: $m/z$ 943.1 [M + H]$^+$ (calc. 943.3). Found C 76.24, H 4.77, N 12.62; C$_{69}$H$_{46}$N$_{10}$S$_2$ requires C 76.79, H 4.30, N 12.98%.

## Compound 11

Solid 4-(bis(4-(7-(diphenylamino)benzo[c][1,2,5]thiadiazol-4-yl) phenyl)amino)benzaldehyde ESI† (50.0 mg, 57.1 μmol) and cyanoacetic acid (10.7 mg, 126 μmol) were added to a flask under an N$_2$ atmosphere. MeCN (60 mL) and a few drops of piperidine were added and the mixture was heated at reflux for 4 days. After cooling, the solvent was removed under reduced pressure and the red residue was purified by column chromatography (SiO$_2$, CH$_2$Cl$_2$ : MeOH 10 : 1). After removal of the solvent, compound **11** was isolated as a red solid (30.0 mg, 31.8 μmol, 56%). $^1$H NMR (500 MHz, DMSO-$d_6$) δ/ppm 8.08 (s, 1H, H$^a$), 8.03 (m, 4H, H$^{D2}$), 7.96 (m, 2H, H$^{C2}$), 7.83 (d, $J$ = 7.8 Hz, 2H, H$^{E5}$), 7.36 (m, 4H, H$^{D3}$), 7.30 (m, 8H, H$^{F3}$), 7.26 (d, $J$ = 7.7 Hz, 2H, H$^{E6}$), 7.12 (m, 2H, H$^{C3}$), 7.07 (m, 4H, H$^{F4}$), 7.01 (m, 8H, H$^{F2}$). $^{13}$C NMR (126 MHz, DMSO-$d_6$) δ/ppm 164.0 (C$^{C=O}$), 154.2 (C$^{E3a}$), 151.1 (C$^{E7a}$), 150.3 (C$^a$), 150.1 (C$^{C4}$), 147.3 (C$^{F1}$), 145.4 (C$^{D1}$), 138.3 (C$^{E7}$), 133.6 (C$^{D4}$), 132.4 (C$^{C1}$), 132.1 (C$^{C2}$), 130.4 (C$^{D2}$), 129.4 (C$^{F3}$), 128.7 (C$^{E5}$), 127.9 (C$^{E4}$), 125.4 (C$^{D3}$), 124.1 (C$^{E6}$), 123.6 (C$^{F2}$), 123.3 (C$^{F4}$), 120.6 (C$^{C3}$), 118.1 (C$^{C\equiv N}$); C$^b$ not resolved. UV-Vis (THF, 1 × 10$^{-5}$ M) λ$_{max}$/nm ($\varepsilon$/dm$^3$ mol$^{-1}$ cm$^{-1}$) 310 (25 600), 328 sh (16 900), 431 (15 300), 482 (16 100). MALDI-TOF MS: $m/z$ 942.1 [M]$^+$ (calc. 942.3). HR ESI-MS negative mode: 941.2470 [M − H]$^-$ (calc. 941.2486). Satisfactory elemental analysis could not be obtained.

## DSC fabrication

DSCs were made using a similar method to that reported.[28] Full details are given in the ESI.†

# Results and discussion

## Ancillary ligand synthesis and characterization

We have recently reported the beneficial effects of incorporating first- or second-generation hole transporting dendrons into the periphery of 2,2′-bipyridine-based copper(I) sensitizers in DSCs,[13] and the use of a co-adsorbant to alleviate steric crowding of these dyes on the semiconductor surface.[16] In this and related work,[12] we have found Hartwig–Buchwald aminations to be a reliable method of coupling diarylamino building blocks to 4-bromophenyl-functionalized 2,2′-bipyridine or 1,10-phenanthroline domains. We have applied an analogous strategy to prepare first generation ligands 3–7 (Scheme 2).[27,28] However, after several attempts to prepare the second generation ligand 8 (Scheme 2) using a Hartwig–Buchwald amination of 4,4′-bis(N,N-diphenylamino)diphenylamine with 4′-(4-bromophenyl)-2,2′:6′,2″-terpyridine, we were unable to isolate a pure product. We therefore turned our attention to the synthesis of the methoxy-decorated ligand 9.

Hartwig–Buchwald amination of 4,4′-bis(N,N-bis(4-methoxyphenyl)amino)diphenylamine[11] with 4′-(4-bromophenyl)-2,2′:6′,2″-terpyridine (Scheme 3) ESI† yielded 9 in 43% yield after workup. The highest mass peak in the electrospray mass spectrum of 9 ($m/z$ = 930.9) was assigned to the [M + H]$^+$ ion, and high resolution ESI MS also confirmed the molecular mass. The $^1$H and $^{13}$C NMR spectra of a THF-$d_8$ solution of 9 were consistent with the $C_2$-symmetric structure shown in Scheme 2, and were assigned by COSY, NOESY, HMQC and HMBC methods. The aromatic region of the $^1$H NMR spectrum is shown in Fig. 2; the methoxy protons give rise to a singlet at δ 3.75 ppm. NOESY cross-peaks between the pairs of protons H$^{B3}$/H$^{C2}$, H$^{C3}$/H$^{D2}$ and H$^{D3}$/H$^{E2}$ (see Scheme 3 for labels) allowed protons in the phenyl rings to be unambiguously assigned. The assignments were confirmed using the HMBC spectrum starting with the high-frequency $^{13}$C NMR signal for C$^{E4}$ (δ 157.1 ppm) which showed a strong correlation to H$^{E2}$, and similarly for cross-peaks C$^{D4}$/H$^{D2}$ and C$^{D1}$/H$^{D3}$.

The synthetic route to compound 10 is summarized in Scheme 4. The secondary amine 10a required for a Hartwig–Buchwald amination with 4′-(4-bromophenyl)-2,2′:6′,2″-terpyridine was prepared starting from the Boc-protected bis(4-bromophenyl)amine. Substitution of the bromo-groups for boronic acid pinacolate esters, followed by a Suzuki coupling[39–41] with two equivalents of 7-(4-bromophenyl)-N,N-diphenylbenzo[c][1,2,5]thiadiazol-4-amine resulted in the formation of the Boc-protected precursor to 10a. Attempts to carry out the deprotection using excess trifluoroacetic acid failed, but heating the Boc-protected precursor[42] at 210 °C in the absence of solvent gave 10a which was used in the Hartwig–Buchwald step without further purification. Compound 10 was isolated as a red solid in 29% yield. The base peak ($m/z$ 943.1) in the MALDI-TOF mass spectrum was assigned to the [M + H]$^+$ ion. The $^1$H and $^{13}$C NMR spectra were assigned using the COSY, NOESY, HMQC and
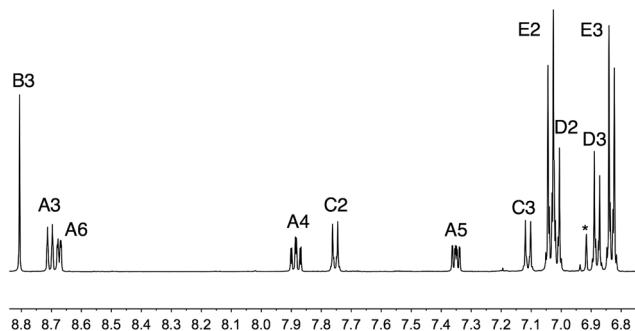
**Fig. 2** The aromatic region of the 500 MHz $^1$H NMR spectrum of **9** in THF-$d_8$ (295 K). See Scheme 3 for atom labelling. * = residual impurity.

HMBC spectra, with NOESY cross-peaks between pairs of protons H$^{B3}$/H$^{C2}$ and H$^{E5}$/H$^{D3}$ allowing unequivocal assignments of the protons in arene rings C, D and E (see Scheme 4).

### Photophysical and electrochemical properties of 9 and 10

The solution absorption spectra of ancillary ligands **9** and **10** are compared in Fig. 3. Compared to the absorption spectrum of 4′-phenyl-2,2′:6′,2″-terpyridine,[43] that of **9** extends into the visible region as a result of the introduction of 4′-(4-(N,N-di(4-methoxyphenyl)amino)phenyl) substituents and consistent with the spectrum of the first generation analogue **4** (Scheme 2). Compounds **4** and **9** exhibit typical intra-ligand charge transfer (ILCT) bands with the tertiary amine functioning as an electron donor.[44] Introduction of the benzothiadiazole unit in **10** extends the spectral response. The broad and intense absorption with $\lambda_{max}$ = 489 nm ($\varepsilon_{max}$ = 26 100 dm$^3$ mol$^{-1}$ cm$^{-1}$) arises from charge transfer[45,46] and the lower energy bands from $\pi^* \leftarrow \pi$ transitions. The spectrum is consistent with those of the related compounds.[45,46]

Compounds **9** and **10** are electrochemically active and cyclic voltammetric (CV) data are presented in Table 1 and in Fig. S1;† processes are reversible unless otherwise stated. The reduction process at −1.96 V in **10** (absent in **9**) arises from reversible reduction of the benzothiadiazole unit.[45,47] The reversible oxidations are centred on the diphenylamine units. Of the



**Fig. 3** Solution absorption spectra of compounds **9**, **10** and **11** in THF (1.0 × 10$^{-5}$ mol dm$^{-3}$).

**Table 1** Cyclic voltammetric data for compounds **9–11** vs. Fc/Fc$^+$ (CH$_2$Cl$_2$) with [$^n$Bu$_4$N][PF$_6$] as supporting electrolyte; scan rate = 0.1 V s$^{-1}$. (ir = irreversible; qr = quasi-reversible)

| Compound | $E^{ox}_{1/2}$/V | $E^{ox}_{1/2}$/V | $E^{ox}_{1/2}$/V | $E^{red}_{1/2}$/V |
|---|---|---|---|---|
| **9** | +0.22 | +0.70$^{qr}$ | +1.06$^{irr}$ | |
| **10** | +0.37 | +0.52 | +0.69 | −1.96 |
| **11** | +0.47 | +0.55 | +0.71 | −1.91 |

oxidations observed for **9** or **10**, the lowest potential process (+0.22 V) is for **9** which is consistent with the presence of the electron-releasing methoxy substituents. In order to support these conclusions, density functional theory (DFT) calculations were run at the B3LYP/6-31G* level. The orbital compositions of the HOMO and LUMO of each of **9** and **10** are shown in Fig. 4. The HOMO in **9** is delocalized over the 4,4′-bis(N,N-bis(4-methoxyphenyl)amino)diphenylamino dendron (Fig. 4a), and the compositions of the HOMO−1 and HOMO−2 are similar (Fig. S2†). The LUMO is based on the tpy domain (Fig. 4b) and the associated reduction process is presumably outside the solvent accessible window. In **10**, the orbital contributions to the HOMO manifold (Fig. 4 and S2†) are similar to those on **9**, and both the LUMO (Fig. 4d) and LUMO+1 are localized on the benzothiadiazole units.

### DSC fabrication and performance

Heteroleptic surface-bound [Zn(L$_{anchor}$)(L$_{ancillary}$)]$^{2+}$ complexes were assembled in a stepwise manner on an FTO/TiO$_2$ electrode using our 'surfaces-as-ligands' strategy.[17,28] The electrode was initially immersed in a DMSO solution of **1** [27] or **2** [48] (Scheme 1), and then the ligand-functionalized electrode was dipped into an EtOH solution of ZnCl$_2$ to give a surface bound [Zn(L$_{anchor}$)Cl$_2$] complex (Fig. 1). Finally, the electrode was dipped for ca. 43 hours in either a CH$_2$Cl$_2$ solution of **9** or a THF solution of **10**, the solvent being chosen according to the solubility of the ancillary ligand. During this dipping cycle, the initially colourless TiO$_2$ layer changed to yellow-orange. The colour persisted when the electrode was dried, consistent with the formation of a surface-bound [Zn(L$_{anchor}$)(L$_{ancillary}$)]$^{2+}$ complex (Fig. 1). We note that the protonation state of surface-bound **1** and **2** is ambiguous and formulation of the dyes as [Zn(**1**)(**9**)]$^{2+}$, [Zn(**1**)(**10**)]$^{2+}$, [Zn(**2**)(**9**)]$^{2+}$ and [Zn(**2**)(**10**)]$^{2+}$ assumes full protonation.

A set of electrodes prepared using TiO$_2$ without a scattering layer was prepared in the same manner as those used in the DSCs, and their solid state absorption spectra were recorded. The spectra of dyes [Zn(**1**)(**9**)]$^{2+}$ and [Zn(**2**)(**9**)]$^{2+}$ are essentially identical, as are those of [Zn(**1**)(**10**)]$^{2+}$ and [Zn(**2**)(**10**)]$^{2+}$ (Fig. 5), consistent with the fact that, above 350 nm, the ancillary ligands dominate the absorption. The beneficial effects of the thiadiazole units are seen in the enhanced absorbance above 400 nm, with maxima at 472 nm for [Zn(**1**)(**10**)]$^{2+}$ and 465 nm for [Zn(**2**)(**10**)]$^{2+}$. These maxima correlate with the charge transfer band at 489 nm in the solution spectrum of ligand **10** (Fig. 3). Fig. 5 also shows the solid-state absorption spectrum of an electrode with adsorbed dye N719, confirming that while the
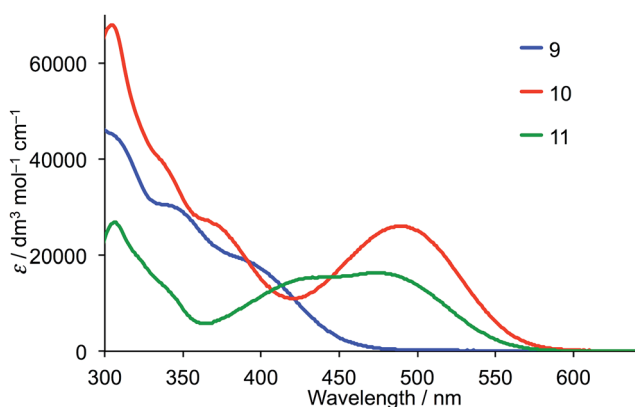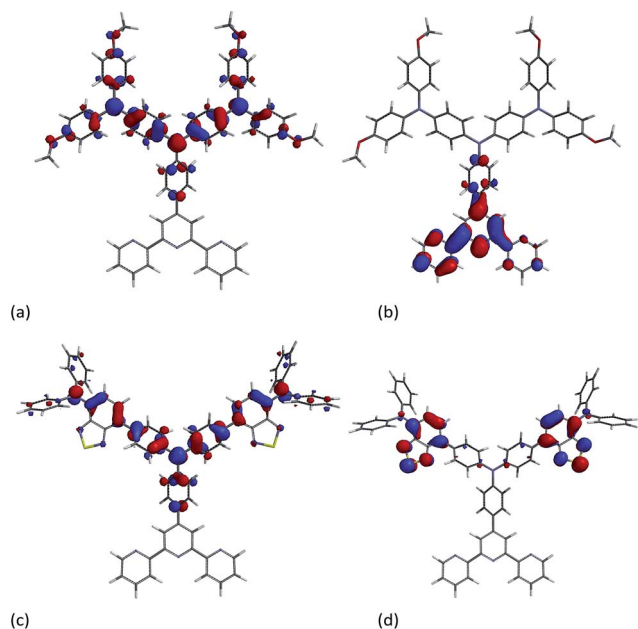
**Fig. 4** Molecular orbital compositions of the (a) HOMO in **9**; (b) LUMO in **9**, (c) HOMO in **10**, and (d) LUMO in **10**.

spectral response of the dyes is enhanced by incorporating the thiadiazole domains, it remains inferior to that of N719.

The DSC measurements were made using sealed and fully masked[49–51] cells with an $I^-/I_3^-$ redox couple. Parameters of cells containing the zinc(II)-based dyes were compared with those of a DSC containing N719 (Table 3 and 4). Duplicate cells were measured for each dye and the efficiencies of the DSCs were remeasured 2, 3 and 10 or 17 days after sealing. External quantum efficiency (EQE) spectra are shown in Fig. 6. For clarity, only the EQE spectrum of the DSC with the highest $EQE_{max}$ for each pair of cells is shown; the same trend in values is observed for both cells, differences falling within the limits of the errors of the measurements. Fig. 7 shows plots of the short-circuit current density ($J_{SC}$) against open-circuit voltage ($V_{OC}$) for DSCs containing $[Zn(\mathbf{1})(\mathbf{10})]^{2+}$ and $[Zn(\mathbf{2})(\mathbf{10})]^{2+}$.
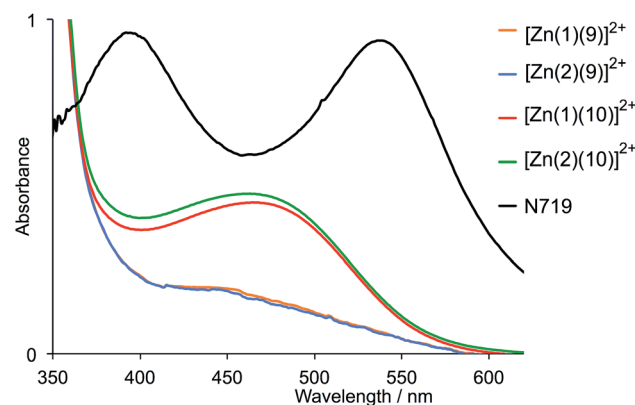
**Fig. 5** Solid-state absorption spectra of FTO/TiO$_2$ electrodes functionalized with the dyes $[Zn(\mathbf{1})(\mathbf{9})]^{2+}$, $[Zn(\mathbf{2})(\mathbf{9})]^{2+}$, $[Zn(\mathbf{1})(\mathbf{10})]^{2+}$, $[Zn(\mathbf{2})(\mathbf{10})]^{2+}$ or N719.

**Table 2** DSC performance of $[Zn(L_{anchor})(\mathbf{9})]^{2+}$. Relative efficiencies are with respect to 100% for N719 measured under the same conditions. Each experiment was measured with two cells (labelled 1 and 2 in the table)

| Anchored dye | Cell | $J_{SC}$/mA cm$^{-2}$ | $V_{OC}$/mV | ff/% | $\eta$/% | Relative $\eta$/% |
|---|---|---|---|---|---|---|
| **On the day of sealing the cell** | | | | | | |
| $[Zn(\mathbf{1})(\mathbf{9})]^{2+}$ | 1 | 0.53 | 380 | 67 | 0.14 | 1.80 |
| $[Zn(\mathbf{1})(\mathbf{9})]^{2+}$ | 2 | 0.55 | 375 | 68 | 0.14 | 1.80 |
| $[Zn(\mathbf{2})(\mathbf{9})]^{2+}$ | 1 | 0.82 | 415 | 68 | 0.23 | 3.00 |
| $[Zn(\mathbf{2})(\mathbf{9})]^{2+}$ | 2 | 0.82 | 408 | 68 | 0.23 | 3.00 |
| N719 | | 17.17 | 635 | 70 | 7.68 | 100 |
| **3 days After sealing the cell** | | | | | | |
| $[Zn(\mathbf{1})(\mathbf{9})]^{2+}$ | 1 | 0.44 | 377 | 69 | 0.11 | 1.38 |
| $[Zn(\mathbf{1})(\mathbf{9})]^{2+}$ | 2 | 0.45 | 374 | 69 | 0.12 | 1.51 |
| $[Zn(\mathbf{2})(\mathbf{9})]^{2+}$ | 1 | 0.81 | 427 | 69 | 0.24 | 3.02 |
| $[Zn(\mathbf{2})(\mathbf{9})]^{2+}$ | 2 | 0.70 | 407 | 67 | 0.19 | 2.39 |
| N719 | | 16.72 | 674 | 71 | 7.94 | 100 |
| **10 days After sealing the cell** | | | | | | |
| $[Zn(\mathbf{1})(\mathbf{9})]^{2+}$ | 1 | 0.43 | 375 | 68 | 0.11 | 1.36 |
| $[Zn(\mathbf{1})(\mathbf{9})]^{2+}$ | 2 | 0.45 | 380 | 69 | 0.12 | 1.48 |
| $[Zn(\mathbf{2})(\mathbf{9})]^{2+}$ | 1 | 0.81 | 428 | 70 | 0.24 | 2.96 |
| $[Zn(\mathbf{2})(\mathbf{9})]^{2+}$ | 2 | 0.71 | 407 | 68 | 0.20 | 2.47 |
| N719 | | 16.71 | 690 | 70 | 8.11 | 100 |

Good fill factors (ff) of *ca.* 70%. were obtained for all the DSCs (Table 2 and 3), but values of $V_{OC}$ are low (*ca.* 400 mV, Table 2 and 3, and Fig. 7). Values of $J_{SC}$ were <1 mA cm$^{-2}$ (compared with 15–17 mA cm$^{-2}$ for N719). The DSCs show very low EQE values (≤3%, Fig. 6), and in contrast to the enhanced absorption of the dyes containing ligand **10** *versus* **9**, the trends in values of $EQE_{max}$ are

**Table 3** DSC performance of $[Zn(L_{anchor})(\mathbf{10})]^{2+}$. Relative efficiencies are with respect to 100% for N719 measured under the same conditions. Each experiment was measured with two cells (1 and 2 in the table)

| Anchored dye | Cell | $J_{SC}$/mA cm$^{-2}$ | $V_{OC}$/mV | ff/% | $\eta$/% | Relative $\eta$/% |
|---|---|---|---|---|---|---|
| **On the day of sealing the cell** | | | | | | |
| $[Zn(\mathbf{1})(\mathbf{10})]^{2+}$ | 1 | 0.52 | 366 | 64 | 0.12 | 1.70 |
| $[Zn(\mathbf{1})(\mathbf{10})]^{2+}$ | 2 | 0.52 | 390 | 67 | 0.13 | 2.02 |
| $[Zn(\mathbf{2})(\mathbf{10})]^{2+}$ | 1 | 0.45 | 396 | 67 | 0.12 | 1.70 |
| $[Zn(\mathbf{2})(\mathbf{10})]^{2+}$ | 2 | 0.46 | 385 | 67 | 0.12 | 1.70 |
| N719 | | 14.93 | 632 | 68 | 6.42 | 100 |
| **3 days After sealing the cell** | | | | | | |
| $[Zn(\mathbf{1})(\mathbf{10})]^{2+}$ | 1 | 0.43 | 385 | 68 | 0.11 | 1.69 |
| $[Zn(\mathbf{1})(\mathbf{10})]^{2+}$ | 2 | 0.43 | 382 | 70 | 0.11 | 1.69 |
| $[Zn(\mathbf{2})(\mathbf{10})]^{2+}$ | 1 | 0.43 | 412 | 70 | 0.13 | 1.99 |
| $[Zn(\mathbf{2})(\mathbf{10})]^{2+}$ | 2 | 0.43 | 388 | 69 | 0.11 | 1.69 |
| N719 | | 14.82 | 646 | 68 | 6.52 | 100 |
| **17 days After sealing the cell** | | | | | | |
| $[Zn(\mathbf{1})(\mathbf{10})]^{2+}$ | 1 | 0.38 | 382 | 70 | 0.10 | 1.62 |
| $[Zn(\mathbf{1})(\mathbf{10})]^{2+}$ | 2 | 0.38 | 383 | 70 | 0.10 | 1.62 |
| $[Zn(\mathbf{2})(\mathbf{10})]^{2+}$ | 1 | 0.40 | 416 | 72 | 0.12 | 1.95 |
| $[Zn(\mathbf{2})(\mathbf{10})]^{2+}$ | 2 | 0.41 | 400 | 70 | 0.11 | 1.72 |
| N719 | | 13.96 | 643 | 69 | 6.15 | 100 |

**Table 4** DSC parameters for blank cell (FTO/TiO$_2$ photoanode). Relative efficiencies are with respect to 100% for N719 measured under the same conditions. Each experiment was measured with two cells

| | $J_{SC}$/mA cm$^{-2}$ | $V_{OC}$/mV | ff/% | $\eta$/% | Relative $\eta$/% |
|---|---|---|---|---|---|
| **On the day of sealing the cell** | | | | | |
| Cell 1 | 0.31 | 460 | 69 | 0.10 | 1.56 |
| Cell 2 | 0.43 | 503 | 71 | 0.16 | 2.50 |
| N719 | 14.93 | 632 | 68 | 6.42 | 100 |
| **3 days After sealing the cell** | | | | | |
| Cell 1 | 0.37 | 474 | 70 | 0.12 | 1.84 |
| Cell 2 | 0.39 | 485 | 71 | 0.13 | 1.99 |
| N719 | 14.82 | 646 | 68 | 6.52 | 100 |

reversed (compare Fig. 5 and 6). This is consistent with the lower values of $J_{SC}$ for the dyes containing ancillary ligand 10 (Table 2 and 3). We rationalize this observation in terms of the positioning of the thiadiazole domain in the ancillary ligand. Although it leads to enhanced absorption in the visible region, its electron-withdrawing effect reduces electron transfer from the ancillary ligand over the metal centre and subsequently reduces electron injection into the TiO$_2$.

The choice of anchoring ligand makes little difference to the performance of the dyes containing ancillary ligand **10**. However, a combination of ancillary ligand **9** with phosphonic acid anchor **2** leads to slightly better dye performance than with carboxylic acid anchor **1** (Table 1). Both $J_{SC}$ and (to a lesser extent) $V_{OC}$ are enhanced on going from carboxylic to phosphonic acid anchor. However, for all the dyes, performance was disappointingly poor, although better than with first generation ancillary ligands **4–7**.[28]

In order to verify the validity of the DSC measurements, parameters of two blank cells (*i.e.* FTO/TiO$_2$ without adsorbed dye) were recorded (Table 4). A comparison of data in Tables 2–4 demonstrates that there are negligible differences between the parameters obtained for the blank cells and some of the DSCs
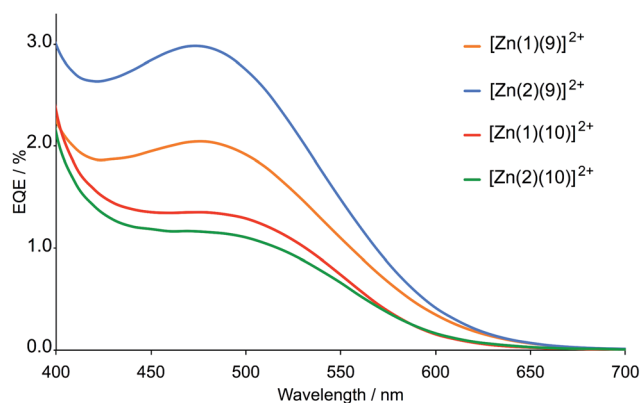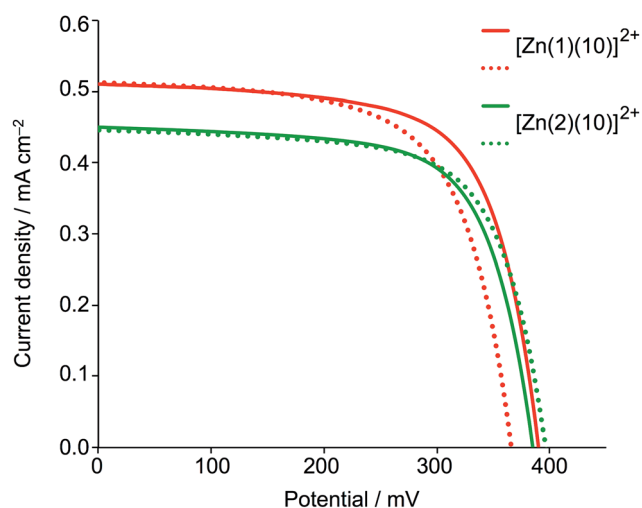
**Fig. 7** $J-V$ curves for duplicate DSCs containing the dyes [Zn(**1**)(**10**)]$^{2+}$ and [Zn(**2**)(**10**)]$^{2+}$ measured on the day of assembling the cells.

containing the zinc(ii) dyes. The results underline the difficulties of measuring parameters for poorly performing sensitizers. However, we note that the EQE spectra of dyes [Zn(**1**)(**9**)]$^{2+}$, [Zn(**2**)(**9**)]$^{2+}$, [Zn(**1**)(**10**)]$^{2+}$ and [Zn(**2**)(**10**)]$^{2+}$ confirm that electron injection (albeit small) does occur. Only for [Zn(**2**)(**9**)]$^{2+}$ was the efficiency higher than the blank cell and this is due to a higher value of $J_{SC}$.

### HOMO and LUMO characteristics of the zinc(ii) dyes

Ground state DFT calculations on the zinc(ii) dyes [Zn(**2**)(**9**)]$^{2+}$ and [Zn(**2**)(**10**)]$^{2+}$ were carried out to gain some insight into their poor DSC performances. In a detailed theoretical study of two representative bis(diimine) copper(i) sensitizers, we demonstrated that the calculated absorption spectra of the dyes depend upon the atomic orbital basis set (6-311++G** basis set on all atoms, 6-311++G** on copper and 6-31G* basis set on C, H and N, or 6-31G* basis set on all atoms) but that the influence on the orbital compositions of the HOMOs and LUMOs are little altered.[52] For a qualitative evaluation of the MOs of [Zn(**1**)(**9**)]$^{2+}$, [Zn(**1**)(**10**)]$^{2+}$, [Zn(**2**)(**9**)]$^{2+}$ and [Zn(**2**)(**10**)]$^{2+}$, we have used a 6-31G* basis set on all atoms.[15]

In their ground state, each of the complexes exhibits a LUMO centred on the anchoring ligand (Fig. 8a and Fig. S3a–S5a†) although it is localized on the tpy domain rather than the carboxylic or phosphonic acid units which would be optimal for electron injection. The HOMO is localized on the peripheral diphenylamino groups of the ancillary ligand (Fig. 8b and Fig. S3b–S5b†) which should facilitate hole-transfer over these domains to the reduced electrolyte. In each complex, the characters of the filled MOs lying immediately below the HOMO are also dominated by contributions from the peripheral groups of the ancillary ligands.

**Fig. 6** EQE spectra of DSCs containing the dyes [Zn(**1**)(**9**)]$^{2+}$, [Zn(**2**)(**9**)]$^{2+}$, [Zn(**1**)(**10**)]$^{2+}$ and [Zn(**2**)(**10**)]$^{2+}$ measured on the day of assembling the cells. For each dye, the DSC exhibiting the higher EQE of the duplicate cells is shown.

### From the zinc(ii) dye containing 10 to organic dye 11

Although the poor performances of the zinc(ii) dyes containing second generation ancillary ligands **9** and **10** were discouraging,
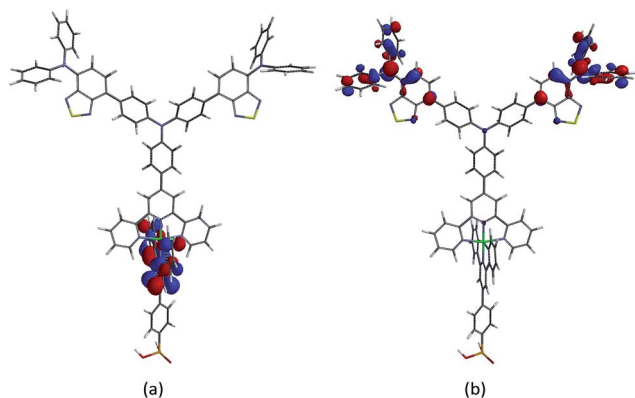
Fig. 8  Molecular orbital compositions in $[Zn(2)(10)]^{2+}$ of (a) the LUMO and (b) the HOMO.

we decided to capitalize on the absorption properties imparted by dendron **10a** by combining this domain with a 2-cyanoacrylic acid anchoring unit to give the organic dye **11** (Scheme 2). Compound **11** was prepared by the route shown in Scheme 5. 4-Bromobenzaldehyde and **10a** were reacted under Hartwig–Buchwald amination conditions, and the resulting aldehyde treated with 2-cyanoacetic acid in the presence of piperidine in a Knoevenagel condensation.[53] Compound **11** was isolated as a red solid in 56% yield.

The highest mass peak envelope in the negative mode high resolution ESI mass spectrum of **11** was observed at $m/z$ 941.2470, consistent with the $[M - H]^-$ ion. The ^{1}H and ^{13}C NMR spectra were assigned using NOESY, COSY, HMQC and HMBC spectra. The 2-cyanoacrylic acid anchoring group was characterized by ^{13}C NMR resonances with the C=O and C≡N groups at $\delta$ 164.0 and 118.1 ppm, respectively. The ^{1}H NMR spectrum is shown in Fig. 9, and is consistent with the presence of the benzothiadiazole units and two generations of amino domains. The cyclic voltammogram of **11** was recorded in $CH_2Cl_2$ and exhibited a reversible reduction at $-1.91$ V; this potential is close to that for the first reduction of **10** (Table 1) and is assigned to a benzothiadiazole-based process. Within the solvent accessible window, compound **11** exhibits three oxidation processes at potentials similar to those for **10** (Table 1) and are, presumably, based on the diphenylamino-containing
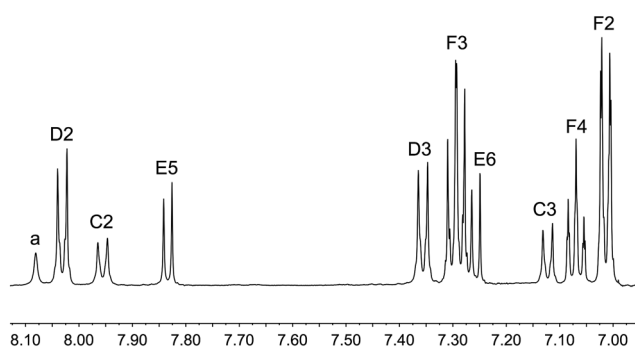
Table 5  DSC performance of **11**. Relative efficiencies are with respect to 100% for N719 measured under the same conditions. Each experiment was measured with two cells

| | $J_{SC}$/mA cm$^{-2}$ | $V_{OC}$/mV | ff/% | $\eta$/% | Relative $\eta$/% |
|---|---|---|---|---|---|
| **On the day of sealing the cell** | | | | | |
| Cell 1 | 10.12 | 613 | 71 | 4.40 | 68.6 |
| Cell 2 | 10.23 | 613 | 71 | 4.48 | 69.8 |
| N719 | 14.93 | 632 | 68 | 6.42 | 100 |
| | | | | | |
| **2 days After sealing the cell** | | | | | |
| Cell 1 | 9.73 | 599 | 72 | 4.21 | 64.6 |
| Cell 2 | 10.16 | 624 | 72 | 4.57 | 70.1 |
| N719 | 14.82 | 646 | 68 | 6.52 | 100 |
| | | | | | |
| **17 days After sealing the cell** | | | | | |
| Cell 1 | 9.04 | 598 | 73 | 3.93 | 63.7 |
| Cell 2 | 9.55 | 610 | 72 | 4.21 | 68.5 |
| N719 | 13.96 | 643 | 69 | 6.15 | 100 |

domains. These assignments are corroborated by the results of the DFT calculations discussed below.

The solution absorption spectrum of **11** (Fig. 3) is dominated by intense high energy bands assigned to $\pi^* \leftarrow \pi$ transitions and a broad CT band with maxima at 431 and 482 nm. The solid-state absorption spectrum of an FTO/TiO$_2$ electrode (which appears bright red by eye) consists of a very broad and intense CT band centred at 460 nm (Fig. S6†) and shows extended spectral response in the red region with respect to the solution absorption (Fig. 3).

Two DSCs incorporating **11** as the sensitizer, and a reference electrode with N719 were fabricated. The performance data in Table 5 confirm the reproducibility of the DSCs and reveal that sensitizer **11** achieves photon-to-current conversion efficiencies that are ≈70% relative to 100% for N719. The $J$–$V$ curves in Fig. 10 demonstrate good fill factors, and high values of both $J_{SC}$ and $V_{OC}$. The DSCs were monitored over a 17 day period and remained stable; no bleaching of the cells was observed. The antenna structure in **11** and the presence of the electron-withdrawing thiadiazole domains contribute to effective
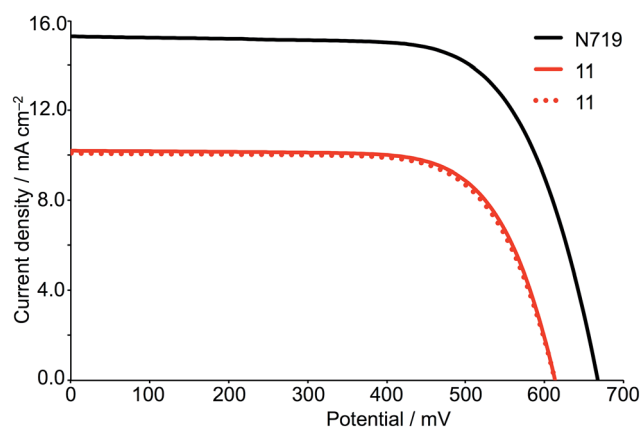


Fig. 9  The 500 MHz ^{1}H NMR spectrum of **11** in DMSO-$d_6$ (295 K). See Scheme 5 for atom labelling.



Fig. 10  $J$–$V$ curves for DSCs containing **11** compared to N719, measured on the day of assembling the cells.
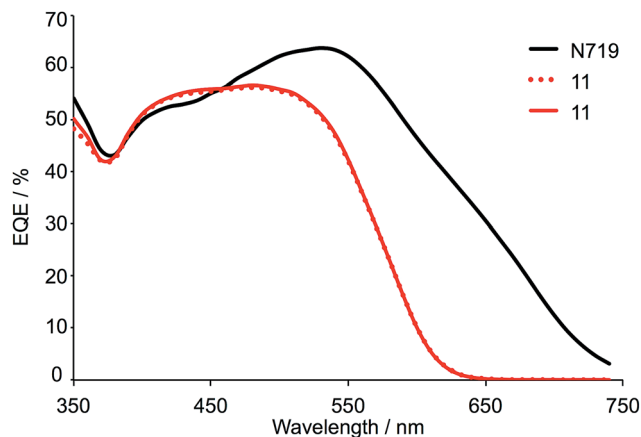
Fig. 11 EQE spectra of DSCs containing **11** compared to N719, measured on the day of assembling the cells.

electronic communication and electron injection. The EQE spectra for the two DSCs containing **11** (Fig. 11) confirm with enhanced electron injection across a broad spectral region. The broad EQE spectrum correlates well with the solid-state absorption spectrum (Fig. S6†). Moving the thiadiazole units closer to the anchoring domain should have beneficial effects and we are currently investigating this and other structural modifications as a means of enhancing dye performance.

### HOMO and LUMO characteristics of organic dye 11

Ground state DFT calculations on **11** reveal that the LUMO and LUMO+1 are close in energy and their combined character is predominantly localized on the 2-cyanoacrylic acid anchoring domain and on the benzothiadiazole groups (Fig. 12a). The HOMO is delocalized as depicted in Fig. 12b, while the HOMO−1 possesses character mainly on the peripheral diphenylamino units. The orbital compositions of the HOMO and LUMO manifolds correspond to what is required, respectively,
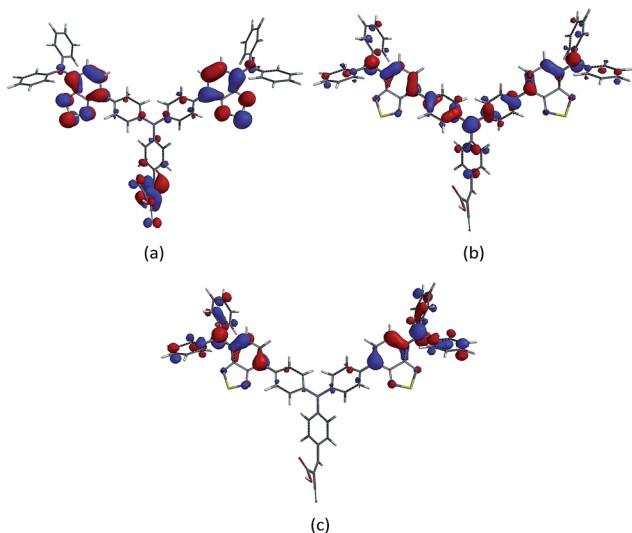
for efficient hole-transfer over the peripheral diphenylamino units to the reduced electrolyte, and localization of the electron on the anchoring domain after excitation. A distinction between the characteristics of the lowest lying virtual MOs in dye **11** and the four zinc(II) complexes is the dominant contribution from the anchor domain in **11** (Fig. 12a) *versus* the localization of the LUMO close to the metal centre in the heteroleptic dyes (Fig. 8a).

## Conclusions

Two tpy ligands **9** and **10** incorporating second-generation diphenylamino-dendrons have been synthesized and characterized. Using the 'surface-as-ligand, surface-as-complex' strategy, the sensitizers $[Zn(\mathbf{1})(\mathbf{9})]^{2+}$, $[Zn(\mathbf{2})(\mathbf{9})]^{2+}$, $[Zn(\mathbf{1})(\mathbf{10})]^{2+}$ and $[Zn(\mathbf{2})(\mathbf{10})]^{2+}$ have been assembled and tested in n-type DSCs. The solid-state absorption spectra of dye-functionalized electrodes confirm a broad spectral response for all the dyes with enhanced intensity for the dyes containing ancillary ligand **10**. A change from the carboxylic acid anchor **1** to phosphonic acid anchor **2** has little effect on light absorption. The dyes perform poorly, with very low $J_{SC}$ and $V_{OC}$. The EQE spectra confirm that $[Zn(\mathbf{1})(\mathbf{9})]^{2+}$ and $[Zn(\mathbf{2})(\mathbf{9})]^{2+}$ exhibit better electron injection than $[Zn(\mathbf{1})(\mathbf{10})]^{2+}$ and $[Zn(\mathbf{2})(\mathbf{10})]^{2+}$. In part, this is probably a consequence of the non-optimal positioning of the thiadiazole domain in the dye. Interpretation of the DSC parameters for this set of dyes highlights a problem that is often ignored when reporting global efficiencies of poor dyes; DSCs incorporating FTO/TiO$_2$ photoanodes *without* adsorbed dye generate small short-circuit current densities and open-circuit voltages which contribute to parameters reported for inefficient dyes.

Organic dye **11** is structurally similar to ancillary ligand **10** and has an excellent spectral response in the range 300–600 nm. EQE data for **11** evidence efficient electron injection over a broad wavelength range, comparable with N719 except above 600 nm. DSCs containing **11** are stable over at least 17 days and show global efficiencies of 3.93–4.57% (*ca.* 70% with respect to N719 set at 100%).

Ground state DFT calculations demonstrate that each of $[Zn(\mathbf{1})(\mathbf{9})]^{2+}$, $[Zn(\mathbf{2})(\mathbf{9})]^{2+}$, $[Zn(\mathbf{1})(\mathbf{10})]^{2+}$, $[Zn(\mathbf{2})(\mathbf{10})]^{2+}$ and **11** possesses a HOMO localized on the peripheral diphenylamino units. In **11**, a dominant contribution from the 2-cyanoacrylic acid anchoring group appears in the lowest lying virtual MOs; in each zinc(II) dye, the LUMO resides on the anchoring ligand but is concentrated on the tpy domain close to the metal centre which may militate against good electron injection.

## Acknowledgements

Fig. 12 Molecular orbital compositions in compound **11** of (a) the summation of LUMO and LOMO+1, (b) HOMO, and (c) HOMO−1.

# Notes and references

1 B. O'Regan and M. Grätzel, *Nature*, 1991, **353**, 737.

2 A. Hagfeldt and M. Grätzel, *Chem. Rev.*, 1995, **95**, 49.

3 S. K. Balasingam, M. Lee, M. G. Kang and Y. Jun, *Chem. Commun.*, 2013, **49**, 1471.

4 H. J. Snaith, *Adv. Funct. Mater.*, 2010, **20**, 13.

5 T. Stergiopoulos and P. Falaras, *Adv. Energy Mater.*, 2012, **2**, 616.

6 G. Boschloo and A. Hagfeldt, *Acc. Chem. Res.*, 2009, **42**, 1819.

7 Z.-S. Wang, K. Sayama and H. Sugihara, *J. Phys. Chem. B*, 2005, **109**, 22449.

8 P. Qin, X. Yang, R. Chen, L. Sun, T. Marinado, T. Edvinsson, G. Boschloo and A. Hagfeldt, *J. Phys. Chem. C*, 2007, **111**, 1853.

9 A. Hagfeldt, G. Boschloo, L. Sun, L. Kloo and H. Pettersson, *Chem. Rev.*, 2010, **110**, 6595.

10 B. Bozic-Weber, E. C. Constable and C. E. Housecroft, *Coord. Chem. Rev.*, 2013, **257**, 3089, and references therein.

11 B. Bozic-Weber, S. Brauchli, E. C. Constable, S. O. Fürer, C. E. Housecroft and I. A. Wright, *Phys. Chem. Chem. Phys.*, 2013, **15**, 4500.

12 B. Bozic-Weber, E. C. Constable, S. O. Fürer, C. E. Housecroft, L. J. Troxler and J. A. Zampese, *Chem. Commun.*, 2013, **49**, 7222.

13 S. Y. Brauchli, B. Bozic-Weber, E. C. Constable, N. Hostettler, C. E. Housecroft and J. A. Zampese, *RSC Adv.*, 2014, **4**, 34801.

14 F. J. Malzner, S. Y. Brauchli, E. Schönhofer, E. C. Constable and C. E. Housecroft, *Polyhedron*, 2014, **82**, 116.

15 F. J. Malzner, S. Y. Brauchli, E. C. Constable, C. E. Housecroft and M. Neuburger, *RSC Adv.*, 2014, **4**, 48712.

16 S. Y. Brauchli, F. J. Malzner, E. C. Constable and C. E. Housecroft, *RSC Adv.*, 2014, **4**, 62728.

17 E. Schönhofer, B. Bozic-Weber, C. J. Martin, E. C. Constable, C. E. Housecroft and J. A. Zampese, *Dyes Pigm.*, 2015, **115**, 154.

18 S. Y. Brauchli, E. C. Constable and C. E. Housecroft, *Dyes Pigm.*, 2015, **113**, 447.

19 M. Sandroni, M. Kayanuma, A. Planchat, N. Szuwarski, E. Blart, Y. Pellegrin, C. Daniel, M. Boujtita and F. Odobel, *Dalton Trans.*, 2013, **42**, 10818.

20 M. Sandroni, M. Kayanuma, M. Rebarz, H. Akdas-Kilig, Y. Pellegrin, E. Blart, H. Le Bozec, C. Daniel and F. Odobel, *Dalton Trans.*, 2013, **42**, 14628.

21 M. Sandroni, L. Favereau, A. Planchat, H. Akdas-Kilig, N. Szuwarski, Y. Pellegrin, E. Blart, H. Le Bozec, M. Boujtita and F. Odobel, *J. Mater. Chem. A*, 2014, **2**, 9944.

22 C. L. Linfoot, P. Richardson, T. E. Hewat, P. Moudam, M. M. Forde, A. Collins, F. White and N. Robertson, *Dalton Trans.*, 2010, **39**, 8945.

23 T. E. Hewat, L. J. Yellowlees and N. Robertson, *Dalton Trans.*, 2014, **43**, 4127.

24 K. A. Wills, H. J. Mandujano-Ramirez, G. Merino, D. Mattia, T. Hewat, N. Robertson, G. Oskam, M. D. Jones, S. E. Lewis and P. J. Cameron, *RSC Adv.*, 2013, **3**, 23361.

25 L. N. Ashbrook and C. M. Elliott, *J. Phys. Chem. C*, 2013, **117**, 3853.

26 M. S. Lazorski and F. N. Castellano, *Polyhedron*, 2014, **82**, 57.

27 B. Bozic-Weber, E. C. Constable, N. Hostettler, C. E. Housecroft, R. Schmitt and E. Schönhofer, *Chem. Commun.*, 2012, **48**, 5727.

28 N. Hostettler, S. O. Fürer, B. Bozic-Weber, E. C. Constable and C. E. Housecroft, *Dyes Pigm.*, 2015, **116**, 124.

29 See for example: M. Schmittel and A. Ganz, *Chem. Commun.*, 1997, 999; M. Schmittel, H. Ammon, V. Kalsani, A. Wiegrefe and C. Michel, *Chem. Commun.*, 2002, 2566.

30 L.-L. Li and E. W.-G. Diau, *Chem. Soc. Rev.*, 2013, **42**, 291.

31 S. Mathew, A. Yella, P. Gao, R. Humphry-Baker, B. F. E. Curchod, N. Ashari-Astani, I. Tavernelli, U. Rothlisberger, M. K. Nazeeruddin and M. Grätzel, *Nat. Chem.*, 2014, **6**, 242.

32 A. Mishra, M. K. R. Fischer and P. Bäuerle, *Angew. Chem., Int. Ed.*, 2009, **48**, 2474.

33 B.-G. Kim, K. Chung and J. Kim, *Chem.–Eur. J.*, 2013, **19**, 5220.

34 H.-H. Chou, Y.-C. Chen, H.-J. Huang, T.-H. Lee, J. T. Lin, C. Tsai and K. Chen, *J. Mater. Chem.*, 2012, **22**, 10929.

35 J.-J. Kim, H. Choi, J.-W. Lee, M.-S. Kang, K. Song, S. O. Kang and J. Ko, *J. Mater. Chem.*, 2008, **18**, 5223.

36 D. H. Lee, M. J. Lee, H. M. Song, B. J. Song, K. D. Seo, M. Pastore, C. Anselmi, S. Fantacci, F. De Angelis, M. K. Nazeeruddin, M. Grätzel and H. K. Kim, *Dyes Pigm.*, 2011, **91**, 192.

37 J. Wang and G. S. Hanan, *Synlett*, 2005, 1251.

38 *Spartan'14*, Wavefunction, Inc., Irvine, CA 92612.

39 J.-J. Kim, H. Choi, J.-W. Lee, M.-S. Kang, K. Song, S. O. Kang and J. Ko, *J. Mater. Chem.*, 2008, **18**, 5223.

40 M. Katono, M. Wielopolski, M. Marszalek, T. Bessho, J.-E. Moser, R. Humphry-Baker, S. M. Zakeeruddin and M. Grätzel, *J. Phys. Chem. C*, 2014, **118**, 16486.

41 R. Misra, P. Gautam and S. M. Mogin, *J. Org. Chem.*, 2013, **78**, 12440.

42 Z. J. Wang, S. Ghasimi, K. Landfester and K. A. I. Zhang, *Chem. Commun.*, 2014, **50**, 8177.

43 T. Mutai, J.-D. Cheon, S. Arita and K. Araki, *J. Chem. Soc., Perkin Trans. 2*, 2001, 1045.

44 K. A. Walters, Y.-J. Kim and J. T. Hupp, *J. Electroanal. Chem.*, 2003, **554–55**, 449.

45 See for example: K. R. Thomas, J. T. Lin, M. Velusamy, Y.-T. Tao and C.-H. Chuen, *Adv. Funct. Mater.*, 2004, **14**, 83.

46 R. Misra and P. Gautam, *Org. Biomol. Chem.*, 2014, **12**, 5448.

47 J.-M. Raimundo, P. Blanchard, H. Brisset, S. Akoudad and J. Roncali, *Chem. Commun.*, 2000, 939.

48 F. C. Krebs and M. Biancardo, *Sol. Energy Mater. Sol. Cells*, 2006, **90**, 142.

49 H. J. Snaith, *Energy Environ. Sci.*, 2012, **5**, 6513.

50 H. J. Snaith, *Nat. Photon.*, 2012, **6**, 337.

51 E. Zimmermann, P. Ehrenreich, T. Pfadler, J. A. Dorman, J. Weickert and L. Schmidt-Mende, *Nat. Photon.*, 2014, **8**, 669.

52 B. Bozic-Weber, V. Chaurin, E. C. Constable, C. E. Housecroft, M. Meuwly, M. Neuburger, J. A. Rudd, E. Schönhofer and L. Siegfried, *Dalton Trans.*, 2012, **41**, 14157.

53 B. List, *Angew. Chem., Int. Ed.*, 2010, **49**, 1730.